PLOS | ONE

RESEARCH ARTICLE

Cullin3 - BTB Interface: A Novel Target for Stapled Peptides

Ivan de Paola[1☯], Luciano Pirone[2☯], Maddalena Palmieri[3], Nicole Balasco[1,3], Luciana Esposito[1,4], Luigi Russo[3], Daniela Mazzà[5], Lucia Di Marcotullio[5], Sonia Di Gaetano[1,4], Gaetano Malgieri[3], Luigi Vitagliano[1,4], Emilia Pedone[1,4]*, Laura Zaccaro[1,4]*

1 Institute of Biostructures and Bioimaging, C.N.R., Napoli, Italy, **2** Institute of Crystallography, C.N.R., Bari, Italy, **3** Second University of Napoli, Caserta, Italy, **4** Interuniversity Centre for Research on Bioactive Peptides (CIRPEB), Napoli, Italy, **5** Department of Molecular Medicine, La Sapienza University, Roma, Italy

☯ These authors contributed equally to this work.
* empedone@unina.it (EP); lzaccaro@unina.it (LZ)

Citation: de Paola I, Pirone L, Palmieri M, Balasco N, Esposito L, Russo L, et al. (2015) Cullin3 - BTB Interface: A Novel Target for Stapled Peptides. PLoS ONE 10(4): e0121149. doi:10.1371/journal.pone.0121149

Academic Editor: Maria Sola, Molecular Biology Institute of Barcelona, CSIC, SPAIN

Received: July 18, 2014

Accepted: February 6, 2015

Published: April 7, 2015

Data Availability Statement: The authors confirm that all data underlying the findings are fully available without restriction. NMR data are available from the Biological Magnetic Resonance Data Bank at http://www.bmrb.wisc.edu/ (Accession Number: 25456 and 25457). The structure of Cul349-68EN has been deposited in the Protein Data Bank at http://www.rcsb.org/pdb/home/home.do (Accession Number: 2myl). The structure of Cul349-68LA has been deposited in the Protein Data Bank at http://www.rcsb.org/pdb/home/home.do (Accession Number: 2mym).

Abstract

Cullin3 (Cul3), a key factor of protein ubiquitination, is able to interact with dozens of different proteins containing a BTB (Bric-a-brac, Tramtrack and Broad Complex) domain. We here targeted the Cul3–BTB interface by using the intriguing approach of stabilizing the α-helical conformation of Cul3-based peptides through the "stapling" with a hydrocarbon cross-linker. In particular, by combining theoretical and experimental techniques, we designed and characterized stapled Cul3-based peptides embedding the helix 2 of the protein (residues 49–68). Intriguingly, CD and NMR experiments demonstrate that these stapled peptides were able to adopt the helical structure that the fragment assumes in the parent protein. We also show that some of these peptides were able to bind to the BTB of the tetrameric KCTD11, a substrate adaptor involved in HDAC1 degradation, with high affinity (~ 300–600 nM). Cul3-derived staple peptides are also able to bind the BTB of the pentameric KCTD5. Interestingly, the affinity of these peptides is of the same order of magnitude of that reported for the interaction of full-length Cul3 with some BTB containing proteins. Moreover, present data indicate that stapling endows these peptides with an increased serum stability. Altogether, these findings indicate that the designed stapled peptides can efficiently mimic protein-protein interactions and are potentially able to modulate fundamental biological processes involving Cul3.

Introduction

Protein-Protein interactions play fundamental roles in living organisms. The ability to modulate these interactions paves the way for the regulation of key physiopathological processes. Different structural elements typically contribute to protein-protein interface. Since these interfaces frequently involve α-helices, peptides mimicking interacting helices represent a valuable tool for modulating protein-protein contacts. However, α-helical regions eradicated from

Funding: This work was funded by the Italian MIUR for financial support (FIRB RBAP114AMK 006). The funders had no role in study design, data collection and analysis, decision to publish, or preparation of the manuscript.

Competing Interests: The authors have declared that no competing interests exist.

their protein context tend to lose their structure, thus limiting the efficacy of the peptide mimetic approaches.

In recent years, different strategies have been developed to stabilize α-helical conformations. By using ring closing metathesis (RCM) developed by Blackwell and Grubbs [1], the Verdine group has optimized α-helix stabilization known as *stapling* introducing synthetic alpha, alpha-di-substituted non-natural amino acids of different lengths and stereochemistries [2]. Although the effectiveness of this stapling approach has been occasionally questioned [3], it has been shown that it can greatly improve the pharmacologic performance of peptides, enhancing their target affinity, resistance toward proteolytic degradation, and serum-half-life, and, most significantly, their cellular uptake [2] thereby increasing the bioavailability and their potential as therapeutic agents. This technology has been already used successfully in different biological contexts [4] such as p53 pathways [5], NOTCH pathways [6], BCL pathways [7], estrogen activation [8], cholesterol efflux [9] and in targeting HIV [10].

In this work the stapling approach has been extended to the interaction of Cullin 3 (Cul3) with proteins containing BTB/POZ (Bric-a-brac, Tramtrack and Broad Complex/Pox virus and Zinc finger) domains. Cul3 is an essential component of the CRL3 system (Cullin 3-Ring ubiquitin Ligases) which facilitates the transfer of ubiquitin to protein substrates [11, 12]. CRL3 is an important regulator of cellular and developmental processes. Its alteration is linked to several human diseases [13]. In performing its function, Cul3 simultaneously binds the Ring protein that carries the E2 enzyme and the substrate adaptor. It has been shown that the Cul3 adaptor partners share a common structural BTB domain [14]. It is important to note that Cul3 is able to interact with dozens of BTB-containing proteins, which potentially bind a variety of different substrates to be ubiquitinated. Therefore, for a large number of proteins, the molecular recognition between Cul3 and BTB domains is a crucial step for protein ubiquitination and regulation. In this scenario, the development of molecules that are able to interfere with Cul3/BTB interaction could represent an important step for regulating a variety of different processes. Here we targeted the interaction of Cul3 with the BTB containing protein KCTD11, one of the best characterized members of the emerging class of multidomain proteins denoted as KCTD (Potassium Channel Tetramerization Domain containing proteins) [15–17]. These proteins present a N-terminal BTB domains which is homologous to the tetramerization domain of voltage-gated K+ (T1) channels. Recent studies have unveiled the crucial role of this class of proteins in important and diversified biological processes i.e. in the insurgence and progression of severe human pathologies including cancer, epilepsy, and obesity [15, 17–23]. It has been shown that some members of the family interact with Cul3 and act as substrate adaptors in the CRL3 system [15, 18, 24–28]. Among them, KCTD11 is an important regulator of the Hedgehog pathway since it works as substrate adaptor for HDAC1 [15]. Previously, we reported that a Cul3-based peptide (residues 49–68 hereafter denoted as $Cul3^{49\text{-}68}$) is able to bind $KCTD11^{BTB}$, despite its rather low structural content as shown by CD characterization[16]. Here we evaluate the impact of stapling on biochemical/biophysical properties of $Cul3^{49\text{-}68}$ derivatives. In particular, we report the design, synthesis, biochemical and structural characterization of novel Cul3-derived peptides obtained through the stapling of different $Cul3^{49\text{-}68}$ regions.

Materials and Methods

Notation

Previous analyses have shown the coexistence of two distinct forms of KCTD11 [17]. The $KCTD11^{BTB}$ domain considered in the present study corresponds to the folded BTB region of the long form (isoform 2 of the UniProt Code Q693B1-2). Accordingly, the numbering of

KCTD11^{BTB} residues used in the text follows this form. Residues of Cul3-derived peptides have been numbered according to their location in Cul3 sequence.

Reagents

TFA, scavengers, DCM, FITC isothiocianate*N*-(+)-biotinyl-6-aminocaproic acid, Grubbs catalyst 1st generation were purchased from Sigma-Aldrich; Novasyn TGR resin, coupling reagents and all amino acids were from Novabiochem. DIPEA was from Romil; piperidine from Biosolve; Fmoc-(S)-2-(4'-pentenyl)alanine was from Boc Science.

Molecular modeling and dynamics

A three-dimensional model of the tetrameric BTB domain of KCTD11^{BTB} (residues 15–116) was generated using standard molecular modeling techniques as implemented in the Swiss Model server (http://swissmodel.expasy.org/) coupled with manual intervention (see supplementary material for details). The crystallographic models of (a) the structure of KCTD5^{BTB} pentamer [23] and (b) the structure of the BTB domain of Akv3.1 voltage-gated potassium channel [29] were used as templates (see supplementary material for details and S1 Fig. for sequence alignments). The complex between the Cul3-based peptide (residues 49–68 of Cul3) and KCTD11^{BTB} was generated by using the structure of the complex between the BTB-containing protein SPOP^{BTB} and Cul3 (PDB code 4EOZ) as template. The final complex (KCTD11^{BTB}-Cul3$^{49-68}$)$_4$ was generated by docking the peptide in the four equivalent binding pockets of KCTD11^{BTB} tetramer.

The energy of this KCTD11^{BTB} model was minimized by using GROMACS software package 4.5.5. GROMACS package was used in the subsequent simulation carried out using (KCTD11^{BTB}-Cul3$^{49-68}$)$_4$ as starting structure. Details about the parameters and the protocol adopted are reported in the supplementary material. To evaluate whether the simulation reached an adequate convergence in the essential space [30], the root mean square inner product (RMSIP) between two halves of the equilibrated trajectory was calculated as described by Di Nola and co-workers [31, 32]. The RMSIP between the first 10 eigenvectors is defined as

$$\sqrt{\frac{1}{10}\sum_{i=1}^{10}\sum_{j=1}^{10}\left(\eta_i^a \eta_j^b\right)^2}$$

Where η_i^a and Z_j^b are the i^{th} and j^{th} eigenvectors from the first and second half of the equilibrated trajectory, respectively.

Peptides synthesis and purification

Cul3$^{49-68}$, Cul3$^{49-68EN}$, Cul3$^{49-68LA}$, Cul3$^{49-68SL}$ and Cul3$^{49-68AA}$ peptides were obtained on solid phase by Fmoc strategy. To mimic the charge status of the fragment within the parent protein, the *N*- and *C*-termini were acetylated and amidated, respectively. The syntheses were carried out with Novasyn TGR resin (substitution 0.25 mmol g^{-1}), using standard Fmoc amino acids and Fmoc-(S)-2-(4'-pentenyl) alanine. Coupling reactions for standard residues were carried out by using 10 equivalents (eq) of Fmoc protected amino acids activated *in situ* with HBTU (9.8 eq)/HOBt (9.8 eq)/DIPEA (20 eq) in DMF for 1 h. Fmoc-(S)-2-(4'-pentenyl)alanine residues were coupled by using 2.5 eq of amino acids and COMU (2.5 eq)/DIPEA (5 eq) in DMF for 6 h.

Fmoc deprotection was performed with 30% piperidine in DMF (10 x 2 min).

Before the cleavage from the resin, the peptides were acetylated, biotinylated or labeled by FITC at *N*-terminus to obtain the corresponding derivatives. The acetylation reaction was carried out using a solution of acetic anhydride (0.5 M)/DIPEA (0.015 M)/HOBt (0.125 M) in DMF (4.7: 4: 91.3 v/v/v) (2 x 15 min). Biotinylated peptides were obtained using a solution of *N*-(+)-biotinyl-6-aminocaproic acid (2 eq)/PyBop (2 eq)/DIPEA (4 eq) in DMF (overnight).

FITC labelling reaction were performed with FITC isothiocianate (2 eq)/ DIPEA 4 (eq) in DMF (overnight).

For ring-closing metathesis, 25 μmol of resin-bound peptide was added to a solution of 20 mM of Grubbs catalyst 1st generation in DCM dry under argon at room temperature (2 x 2 h). The reaction was monitored by ESI-LC-MS instrument, (ThermoFinnigan, NY, USA) equipped with a diode array detector combined with an electrospray ion source and ion trap mass analyzer, using a Phenomenex Jupiter Proteo column (150 × 2 mm; 4 μm; 90 Å) and a linear gradient of H_2O (0.1% TFA)/CH_3CN (0.1% TFA) from 20 to 80% of CH_3CN (0.1% TFA) in 15 min at flow rate of 200 μL/min.

All peptides were cleaved off the resin by treatment with a mixture of TFA/H_2O/EDT/TIS (94:2.5:2.5:1 *v/v/v/v*) for 3 h at room temperature. The resins were filtered and the crude peptides were precipitated with diethyl ether, dissolved in H_2O/CH_3CN mixture (1: 1 *v/v*) and lyophilized. The peptides were purified by preparative RP-HPLC on the Shimadzu system equipped with a UV-Vis detector SPD10A using a Phenomenex Jupiter Proteo column (21.2 × 250 mm; 4 μm; 90 Å) and a linear gradient of H_2O (0.1% TFA)/CH_3CN (0.1% TFA) from 20 to 80% of CH_3CN (0.1% TFA) in 30 min at flow rate of 20 mL/min. The collected fractions containing the desired compounds were lyophilized. The identity and purity of all peptides were assessed by LC-MS. The final yields of $Cul3^{49-68}$ and stapled peptides were 25%. Fluorescent and biotinylated derivatives were obtained with a final yield of about 20%.

Protein expression and purification

$KCTD11^{BTB}$ was expressed as a recombinant fusion protein with thioredoxin A (TrxA). The expression and purification were performed as previously described [17]. The protein, extensively dialysed against 20 mM phosphate buffer pH 7.5, 150 mM NaCl, was used for different purposes. The pET28/$KCTD5^{BTB}$ plasmid was a gift of Prof. Goldstein (University of Chicago). $KCTD5^{BTB}$, corresponding to the folded BTB domain of KCTD5 (residues 44–145), was expressed and purified as elsewhere reported [33, 34].

Circular dichroism spectroscopy studies

Far-UV CD spectra were collected on a Jasco J-810 spectropolarimeter from 190 to 260 nm at 25° C using a quartz cell with of 0.1-cm path length. The spectra were acquired using the following parameters: 0.5 nm step resolution, 10 nm/min scanning speed, 8s response time and 1 nm spectral band width. The spectra were recorded at peptide concentration ranging from 10 to 90 μM, at pH 3.0 (0,1% TFA) and at pH 7.0 (10 mM phosphate buffer). The final spectra were expressed as molar ellipticity θ (deg cm^2 $dmol^{-1}$) *per* residue. Deconvolutions of CD spectra were obtained using the CONTINLL program, which is part of the web-based program CdPro (http://lamar.colostate.edu/~sreeram/CDPro/).

ELISA assay

For ELISA assays, 5 μg/mL streptavidin in phosphate/citrate buffer pH 5.0 was incubated overnight at 37°C for coating. Firstly, wells were coated with 0.8 μM biotinylated $Cul3^{49-68}$ peptides in phosphate buffered saline (PBS) 1X for 1 h at room temperature. Binding step was performed with increasing concentrations (0.4, 0.75, 1.5, 3.8, 7.6 and 15.6 μM) of His-TrxA-

KCTD11^{BTB} in PBS 1X. His-TrxA was used as negative control in the same concentrations. As blocking solution 3% gelatine, 0.05% Tween-20 in PBS 1X was used for 1 h at 37°C. Washes were executed with PBS 1X. To reveal the occurred interaction mouse anti-His monoclonal antibody was incubated in 1:1000 dilution at room temperature for 2 h; then, horseradish peroxidase-conjugated anti-mouse antibody (Pierce) was diluted 1:10000 in 1% gelatin, PBS 1X and incubated at 20°C for 1 h. The colorimetric reaction has been carried out with SIGMAFAST OPD reagent (Sigma Aldrich), according to the manufacturer's instructions. Finally, a Model 680 Microplate Reader (Bio-Rad, Hercules, CA-USA) has been used for readings at 490 nm; data were processed by a Microplate Manager 5.2 program. The reported data are mean values of triplicate experiments.

Fluorescence polarization

Polarization measurements were conducted using a Synergy 2 Multi-Mode Microplate Reader (BioTek) with the fluorescence polarization module. Excitation wavelength was 460 ± 40 nm and emission was detected at 528 ± 20 nm. For each independent experiment a concentration of 2 μM of FITC- Cul3$^{49\text{-}68}$ peptides was used. The final volume per well in 384-well plate format was 60 μl. Binding assays were performed adding KCTD11^{BTB} at increasing concentration (from 0.1 μM to 15 μM) [35]. Analogous experiments were conducted on KCTD5^{BTB},expressed and purified as previously described [33]. Binding curves were generated and dissociation constants (K_D) were calculated from the nonlinear regression curve using GraphPad Prism and the following equation [35]:

$$FP - FP_0 = B_{MAX} * \frac{[KCTD11^{BTB}]}{(K_D + [KCTD11^{BTB}])}$$

in which FP is the fluorescence polarization (measured in mP), [KCTD11^{BTB}] is the molar concentration of KCTD11^{BTB} as monomer, Bmax is the maximum polarization, and FPzero is a correction factor to account for the intrinsic polarization of the peptide evaluated in each experiment. A competition experiment with the unlabeled peptide (Cul3$^{49\text{-}68LA}$) was performed.

Nuclear magnetic resonance spectroscopy

NMR samples of Cul3$^{49\text{-}68}$, Cul3$^{49\text{-}68EN}$, Cul3$^{49\text{-}68LA}$ were dissolved in 500 μl of a water solution containing 0.1% TFA and 50 μl of D_2O adjusted at pH = 3. All of the NMR experiments were acquired on a Varian Unity INOVA 500 MHz spectrometer.

A standard set of 2D experiments, TOCSY [36] and NOESY [37] were acquired at 25°C. The TOCSY experiments were recorded using a mixing time of 70 ms while the NOESY spectra were carried out with a mixing time of 300 ms. Chemical shifts were referenced to external TMS (tetramethylsilane) (δ = 0 ppm).

NMR data were processed by using Varian (VNMR6.1B) software and analyzed and assigned using XEASY program [38]. Chemical shift deviations of H^{α} protons for Cul3$^{49\text{-}68}$, Cul3$^{49\text{-}68EN}$ and Cul3$^{49\text{-}68LA}$ were estimated by using as references random coil H^{α} chemical shift values [39].

The structure of the peptides were calculated using CYANA [40]. The upper limits of the distance restraints were obtained from the NOESY cross-peak intensities using the calibration routine of CYANA. During the CYANA runs, the peptides were calculated with and without the olefinic linker, and the non-standard amino acid (S)-2-(4'-pentenyl) alanine was added in the cyana library. The structures were analyzed and visualized by using the program MOLMOL [41] and PROCHECK [42].

The dihedral angles were estimated using HN and Hα chemical shifts by the software PREDITOR[43]. The secondary structure propensity has been evaluated based on the HN and Hα chemical shifts using the software Secondary Structure Propensity (SSP)[44].

Serum stability

Human serum (Sigma Aldrich-Italy) was centrifuged at 13000 rpm for 10 min to remove lipids;the supernatant was collected and incubated at 37°C for at least 15 min. The assay started upon the addition of the peptides to the 25% serum for a final peptide concentration of 0.3 μM.

200 μL aliquots of the samples were taken after the following time points: 0, 60, 120, 180, 360 and 900 min. The aliquots were mixed with 100 μL of 15% TFA and incubated at 4°C for at least 15 min to induce the precipitation of the serum proteins. The supernatants were collected for each sample after centrifugation at 13000 rpm for 10 min and stored at -20°C.

The serum stability of peptides was followed by LC-MS analysis. using a Phenomenex Jupiter C4 (150 × 2 mm; 5 μm; 300 Å) and a method consisting of an isocratic step with H2O (0.1% TFA)/CH3CN (0.1% TFA) (70:30) for 10 min and a linear gradient of H_2O (0.1% TFA)/CH_3CN (0.1% TFA) from 30 to 80% of CH_3CN (0.1% TFA) in 20 min at flow rate of 200 μL/min.

The assays were performed in triplicate.

Results

KCTD11—Cul3 recognition and peptide design

In order to design variants of the peptide with improved $Cul3^{49-68}$ biochemical/biophysical properties, we preliminarily investigated the mechanism of molecular recognition between KCTD11 and $Cul3^{49-68}$. Previous investigations have shown that $KCTD11^{BTB}$ adopts a tetrameric structure [17]. Therefore, we generated a homology model of the $KCTD11^{BTB}$ tetramer based on the structure of two related proteins (i) the voltage-gated potassium channel Akv3.1 [29] and (ii) KCTD5 [23] (see materials and methods for details). Notably, the most important residues involved in the interactions formed at Akv3.1 tetramer interface (Asp56 and Arg70) are conserved in KCTD11 sequence (Asp66 and Arg80). Indeed, the inspection of the subunit interface indicates that the electrostatic interactions that stabilize $KCTD11^{BTB}$ tetramer are similar to those found for Akv3.1. The main difference between the model of tetrameric $KCTD11^{BTB}$ and Akv3.1 is the orientation of the α5 helix located at the very C-terminal end of the domain. In the BTB domain of Akv3.1 this helix, which is deeply involved in the coordination of Zn ion, folds against the rest of the protein. In $KCTD11^{BTB}$ the C-terminus of this helix protrudes toward the solvent (Fig. 1). It is likely that the location of α5 promotes the correct relative orientation between $KCTD11^{BTB}$ and the C-terminal substrate-binding domain of the protein, which is involved in the recognition process of HDAC1 [15], whose structure is hitherto unknown.

The model for the tetrameric association between $KCTD11^{BTB}$ and $Cul3^{49-68}$ was generated using the structure of the complex between Cul3 and $SPOP^{BTB}$ as template (see materials and methods for details). The modeling indicates that $Cul3^{49-68}$ binds $KCTD11^{BTB}$ in a cavity located at the tetramer interface (Fig. 1). In order to gain further data about $Cul3^{49-68}$-$KCTD11^{BTB}$ recognition process, the structure of the complex was used as a starting model in molecular dynamics studies.

In line with previous binding experiments [16], the analysis of the $(KCTD11^{BTB}\text{-}Cul3^{49-68})_4$ assembly during the simulation indicates that structures reach a rather stable state in the 30–130 ns interval of the simulation (S2 Fig.). This is evident from the analysis of the RMSD values and the gyration radius. Moreover, the RMSIP value computed on two independent halves of

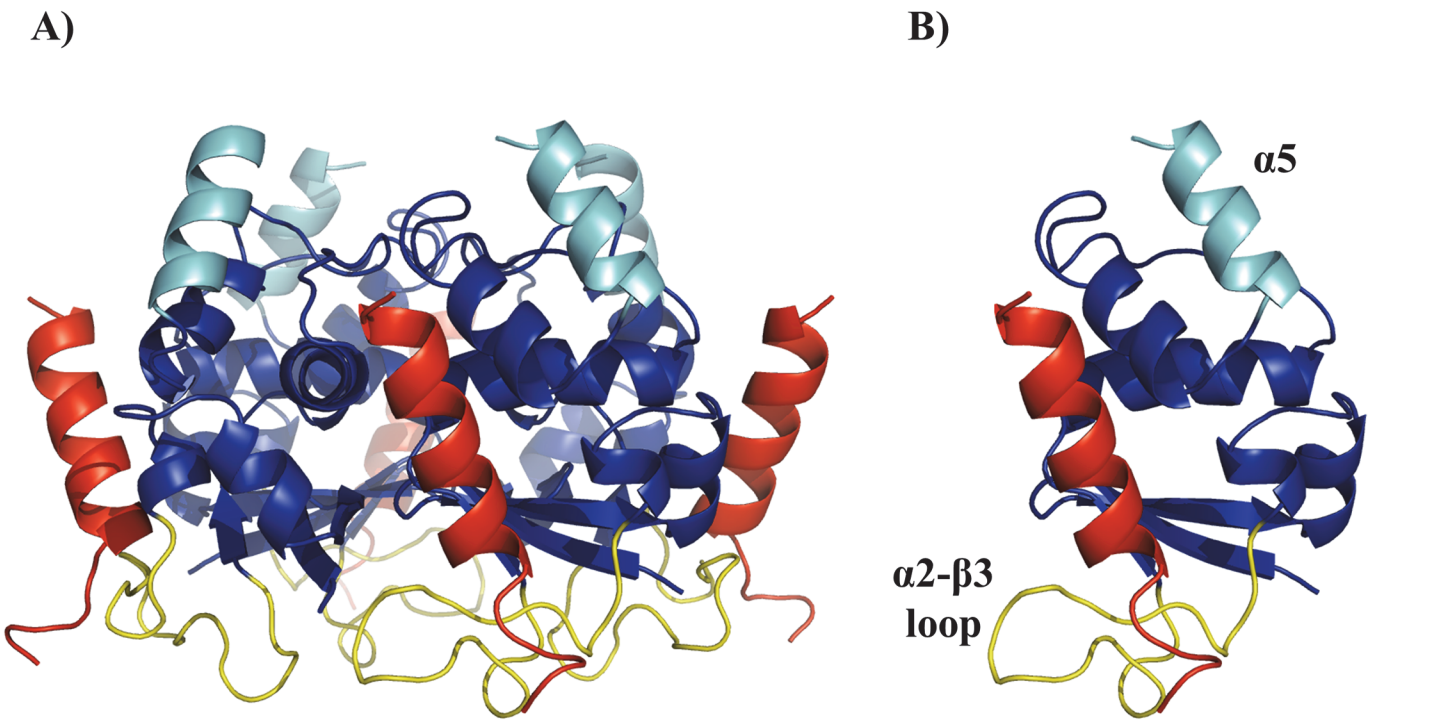

Fig 1. Three-dimensional model of the complex (KCTD11^{BTB}-Cul3$^{49-68}$)$_4$. (A) The model of the three-dimensional structure of the complex (KCTD11^{BTB}-Cul3$^{49-68}$)$_4$ that was used as starting model in the molecular dynamics simulation. The peptide Cul3$^{49-68}$ is coloured in red. The C-terminal helices (α5) which protrude toward the solvent and the interacting loop α2-β3 of the four KCTD11^{BTB} chains are shown in cyan and yellow, respectively. (B) A snapshot of a monomer KCTD11^{BTB}-Cul3$^{49-68}$ which highlights the location of key elements of the model is reported.

doi:10.1371/journal.pone.0121149.g001

the trajectory was 0.65 (see supplementary material for details).This indicates that an adequate convergence of the simulation was achieved.

The evaluation of the protein and the peptide dynamics throughout the trajectory, carried out through the analysis of the root mean square fluctuation (RMSF) values calculated on C$^{\alpha}$ atoms in the equilibrated region of the trajectory, suggests that structured regions of KCTD11^{BTB} are rather rigid (RMSF ~1.0 Å) (S3A Fig.). Nevertheless, RMSF values increase up to 4. Å for loop and terminal regions. Very high RMSF values are displayed by the α2-β3 loop, which is believed to play a significant role in BTB Cullin recognition. With the exception of the terminal ends, Cul3$^{49-68}$ also displays rather low RMSF values that often are below 2.0 Å (S3B Fig.). The relative rigidity of Cul3$^{49-68}$ is confirmed by the monitoring of the secondary structure content of the peptide along the trajectory. Indeed, the peptide retains a significant level of secondary structure throughout the simulation, despite some local unfolding observed at the C-terminus of the helix (S4 Fig.). The analysis of the buried area of the peptide residues upon complex formation clearly indicates that aromatic residues are deeply involved in intermolecular interactions (Fig. 2). Indeed, the largest buried areas correspond to the residues Phe54, Tyr58 and Tyr62, which are located on the same side of the helix. This observation is corroborated by the analysis of specific interactions that are preserved in the simulations (S5 Fig.). Most conserved ones are those established by residues of the regions α2-β3 and α4-α5 of KCTD11^{BTB} and the aromatic residues Tyr58 and Tyr62 of Cul3$^{49-68}$. These include both hydrogen bonding and hydrophobic interactions established by aromatic side chains.

Overall these findings indicate that the helicity of the peptide represents a major requirement for its efficient binding to KCTD11^{BTB}. However, solution studies demonstrate that Cul3$^{49-68}$ presents a very low intrinsic propensity to adopt this kind of structure [16]. To

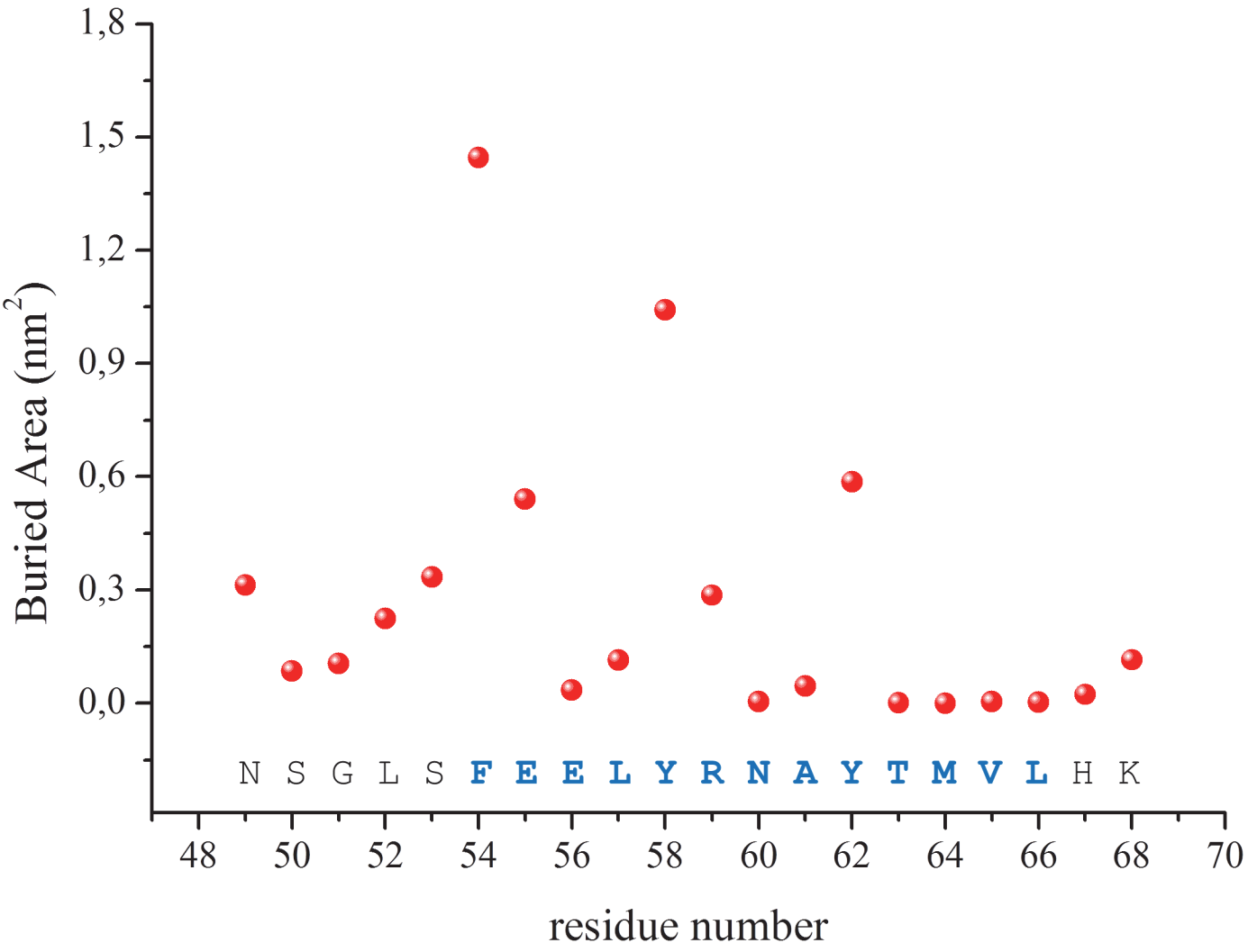

Fig 2. Buried area of Cul3$^{49\text{-}68}$ residues upon complex formation with KCTD11^{BTB}.

doi:10.1371/journal.pone.0121149.g002

evaluate the effect of an increase of the helical propensity of the peptide biochemical/biophysical properties we planned to incorporate an all-hydrocarbon "staple" into this peptide. Since it has been shown that the extent of α-helix stabilization provided by stapling is substantially context dependent [3], we used the results of the MD analysis to design Cul3-derived stapled peptides. The analysis of the buried area of Cul3$^{49\text{-}68}$ residues on KCTD11 (Fig. 2) binding suggests that residues Tyr58 and Arg59 are surrounded by completely solvent-exposed residues (Glu56, Leu57, Asn60 and Ala61). In this scenario, staples encompassing one turn of the helix (residues *i* and *i+4*), such as those obtained through the replacement of the pair Glu56-Asn60 or alternatively Leu57-Ala61, were expected to produce minimal perturbation of the binding site between the protein and the peptides. Therefore, we designed two stapled variants of Cul3$^{49\text{-}}$68 in which either Glu56-Asn60 (denoted as Cul3$^{49\text{-}68EN}$) or Leu57-Ala61 (Cul3$^{49\text{-}68LA}$) were replaced with the non-standard amino acid (S)-2-(4'-pentenyl) alanine (S5). Moreover, we also characterized the mutant Cul3$^{49\text{-}68AA}$, a non-stapled variant in which Tyr58 and Tyr62 were replaced with Ala residues. Since Phe54 side chain is buried upon complex formation, we also designed a staple by replacing the pair Ser53-Leu57 (Cul3$^{49\text{-}68SL}$) with the aim to increase

Ac–NSGLSFEELYRNAYTMVLHK–NH2	$Cul3^{49-68}$
Ac–NSGLSFEES_5YRNS_5YTMVLHK–NH2	$Cul3^{49-68LA}$
Ac–NSGLSFES_5LYRS_5AYTMVLHK–NH2	$Cul3^{49-68EN}$
Ac–NSGLS_5FEES_5YRNAYTMVLHK–NH2	$Cul3^{49-68SL}$
Ac–NSGLSFEELARNAATMVLHK–NH_2	$Cul3^{49-68AA}$

Fig 3. Aminoacid sequences of all peptides. The replaced residues are highlighted in red. S_5 corresponds to the non-standard amino acid (S)-2-(4'-pentenyl) alanine.

doi:10.1371/journal.pone.0121149.g003

the local helicity of the peptide, although this region is not fully structured in Cul3 where the helix spans from residue 54 to 66. The sequences of the peptides that have been characterized are reported in Fig. 3.

Circular dichroism characterization of stapled peptides

Although detailed structural data on these peptides were obtained by NMR (see below), preliminar insights into the structural preferences of the peptides considered in the present study were gained by far-UV CD experiments. The spectra were registered in 10 mM phosphate buffer at pH 7.0. In line with a previous characterization of the peptide [16], the CD spectrum indicates that $Cul3^{49-68}$ presents a very limited structural content (Fig. 4). Notably, all stapled peptides exhibit an increased amount of helical structure as indicated by the positive peak at wavelength of ~ 190 nm and the two negative peaks at about 210 and 222 nm. The intensity of the positive peak and the location of the negative ones suggest that $Cul3^{49-68SL}$ is endowed with slightly lower secondary structure content. Indeed, the ratios of disordered/helical structural contents were estimated to be 3.98, 1.95, 1.72 and 0.93 for $Cul3^{49-68}$, $Cul3^{49-68\ SL}$, $Cul3^{49-68EN}$ and $Cul3^{49-68\ LA}$, respectively. This finding confirms that these peptides have different helical propensities. The CD spectra were also collected at pH 3.0 for all peptides. They were roughly identical to those collected at pH 7.0 (S6 Fig.). No concentration effects were observed on the shape and intensity of the spectra in the range (10^{-6}-10^{-5} M) taken into consideration.

Affinity

The ability of the peptides to bind recombinant $KCTD11^{BTB}$ was qualitatively checked by ELISA (Fig. 5). $Cul3^{49-68}$, $Cul3^{49-68EN}$ and $Cul3^{49-68LA}$ resulted to be able to bind $KCTD11^{BTB}$ with a comparable affinity as highlighted by the trend of ELISA assays (Fig. 5). On the other hand, $Cul3^{49-68SL}$ showed a greatly reduced affinity. No relevant binding was detected for $Cul3^{49-68AA}$. To obtain a quantitative estimate of the dissociation constants of the most affine binders, $Cul3^{49-68}$, $Cul3^{49-68EN}$ and $Cul3^{49-68LA}$, fluorescence polarization experiments were carried out (Fig. 6 and S7 Fig.). The fitting of data gave the following K_D values: 497 ± 127 nM, 620 ±177 nM and 305 ± 100 nM for $Cul3^{49-68}$, $Cul3^{49-68EN}$ and $Cul3^{49-68LA}$, respectively. A possible contribution of the fluorophore FITC to the binding to $KCTD11^{BTB}$ was excluded by a competition experiment with unlabeled $Cul3^{49-68LA}$ (S8 Fig.).

Moreover, the fluorescence polarization experiment was also extended to the pentameric $KCTD5^{BTB}$. This experiment demonstrates that $Cul3^{49-68LA}$ is able to interact also with this domain (97±20nM) (Fig. 7). Interestingly, $Cul3^{49-68LA}$ recognizes BTB domains endowed with different oligomeric organization with a high affinity.

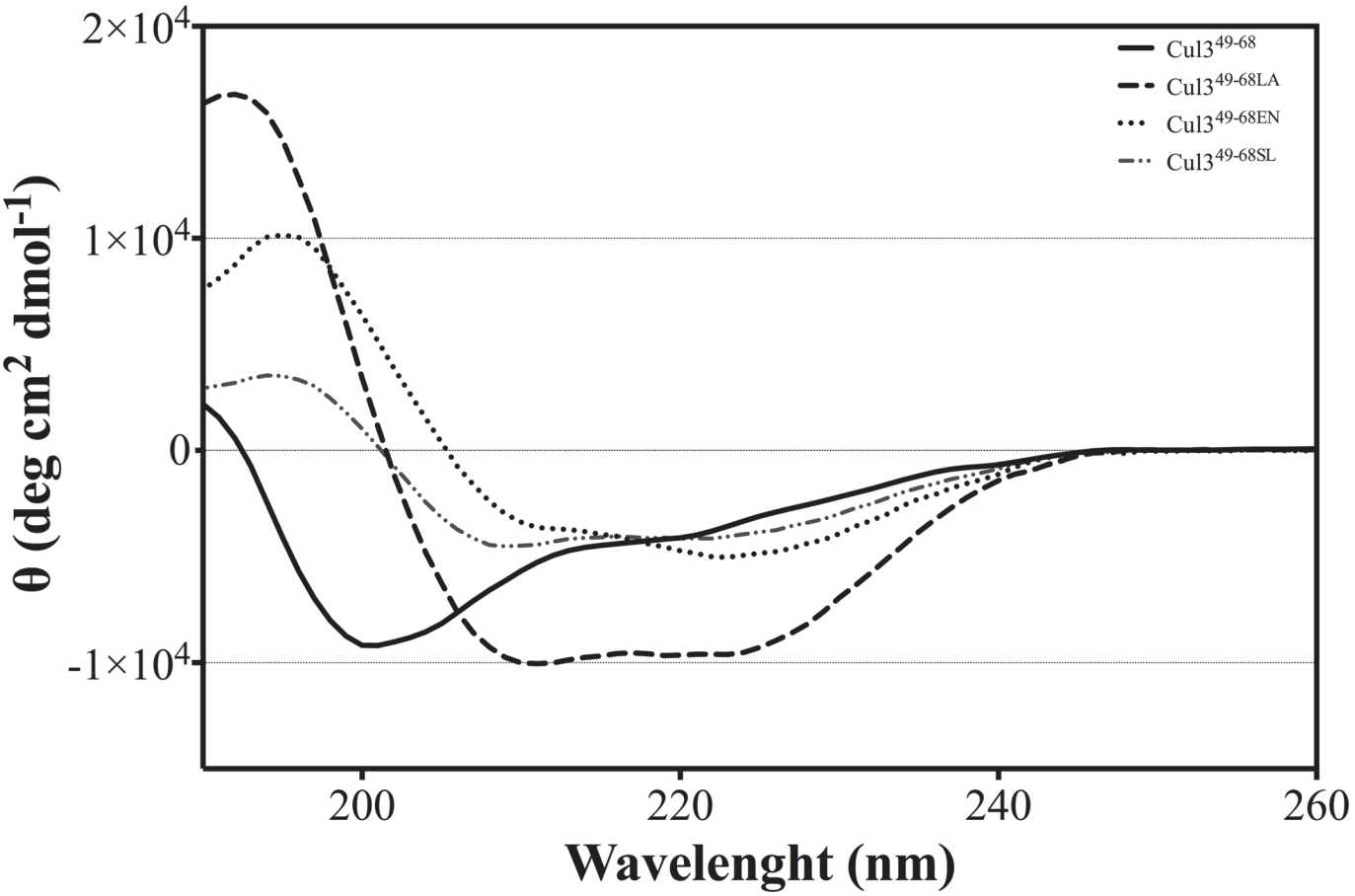

Fig 4. CD spectra. Far-UV CD spectra of Cul3$^{49\text{-}68}$, Cul3$^{49\text{-}68EN}$, Cul3$^{49\text{-}68LA}$, and Cul3$^{49\text{-}68SL}$. Spectra were acquired in 10 mM phosphate buffer pH 7.0.

doi:10.1371/journal.pone.0121149.g004

NMR structure

NMR measurements for the Cul3$^{49\text{-}68}$ peptide have been carried out at pH 3.0. These conditions have been chosen as this peptide has shown a tendency to aggregate at the NMR concentrations upon increasing the pH value. The complete assignment of the ^{1}H resonances has been obtained (for chemical shifts see S1 Table). The narrow range of the HN resonances dispersion and the absence of secondary structure diagnostic NOEs clearly indicate that Cul3$^{49\text{-}68}$ does not assume a definite conformation in these conditions, in agreement with the far-UV CD results. Nevertheless, due to their sensitivity to the chemical environment, the deviations of the Hα chemical shifts with respect to their random coil values (Fig. 8) demonstrate a slight tendency of the peptide to assume a helical conformation, reflecting the helical nature of the sequence 54–66 in the parent protein.

The NMR spectra for the stapled peptides (Cul3$^{49\text{-}68EN}$ and Cul3$^{49\text{-}68LA}$) have been carried out in the same conditions obtaining the complete assignment of their resonances. As expected, the HN resonances dispersion and the analysis of the observed Hα chemical shift deviations for both stapled peptides indicate that the incorporation of two (S)-2-(4'-pentenyl)alanine modified amino-acids into the Cul3$^{49\text{-}68}$ sequence results in a net increase of α-helical content (S2 and S3 Tables). On the contrary, in the case of Cul3$^{49\text{-}68SL}$ peptide, the NMR spectrum indicates that the introduction of the stapling bridge in these positions does not significantly improve the helical content (S9 Fig.).

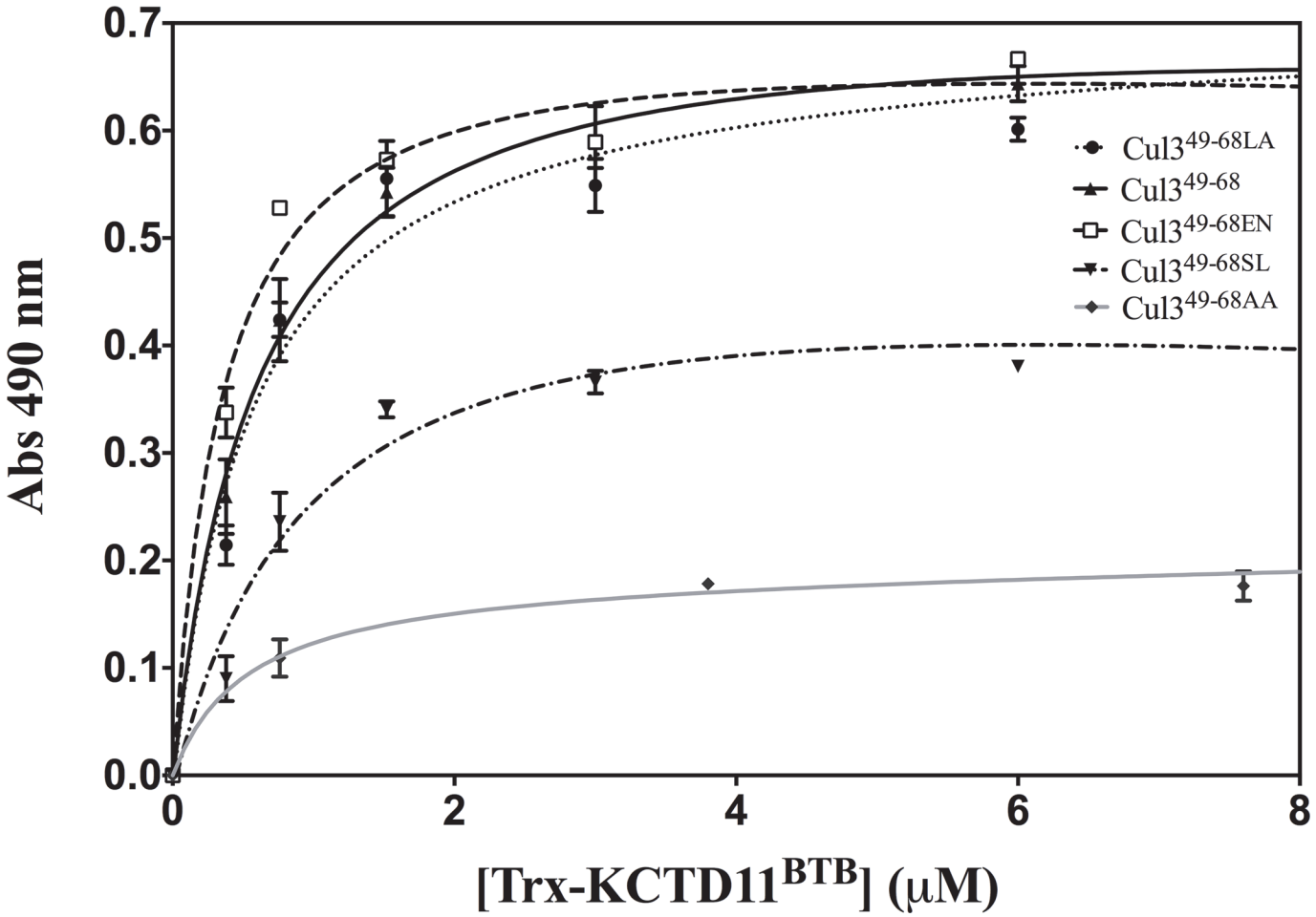

Fig 5. ELISA assays. Binding curves obtained from ELISA on KCTD11^{BTB} using the biotinylated peptides Cul3$^{49\text{-}68}$ (▲),Cul3$^{49\text{-}68LA}$ (●),Cul3$^{49\text{-}68EN}$ (■), Cul3$^{49\text{-}68SL}$ (▼) and Cul3$^{49\text{-}68AA}$(◆).

doi:10.1371/journal.pone.0121149.g005

The good quality of the spectra and the good number of NOE cross peaks encouraged us to calculate the structure of Cul3$^{49\text{-}68EN}$ and Cul3$^{49\text{-}68LA}$ peptides. At first, we predicted the secondary structure content of both peptides based on the Hα and HN chemical shifts using the Chemical Shift Index method [45]. Moreover, the helical content was further confirmed by the analysis of the predicted φ and ψ angles (S4 and S5 Tables) and the secondary structure propensity for each residue of both peptides was also evaluated (S10A and B Fig.). The structures were calculated based on 218 and 214 experimental NOE derived distance constraints respectively (Figs. 9 and 10).

The ensemble of the 20 best structures of Cul3$^{49\text{-}68EN}$ and Cul3$^{49\text{-}68LA}$ show a backbone r.m.s.d. of 0.159Å (residues 52–66) and 0.154 Å (residues 52–66) and an average target function of 0.84 ± 0.03 and 0.63 ± 0.02 respectively. There were no distance violations greater than 0.2 Å and no dihedral violations greater than 5°. The structural statistics of the 20 best structures for the two stapled peptides are reported in Figs. 9 and 10.

Both Cul3$^{49\text{-}68EN}$ and Cul3$^{49\text{-}68LA}$ peptides adopt an extensive helical conformation (Figs. 9 and 10) that allows the three aromatic residues playing a crucial role in the recognition mechanism of these peptides (Phe54, Tyr58 and Tyr62) residing in the same face of the helix. The two structures are however slightly different. In particular, Cul3$^{49\text{-}68LA}$ α-helix encompasses

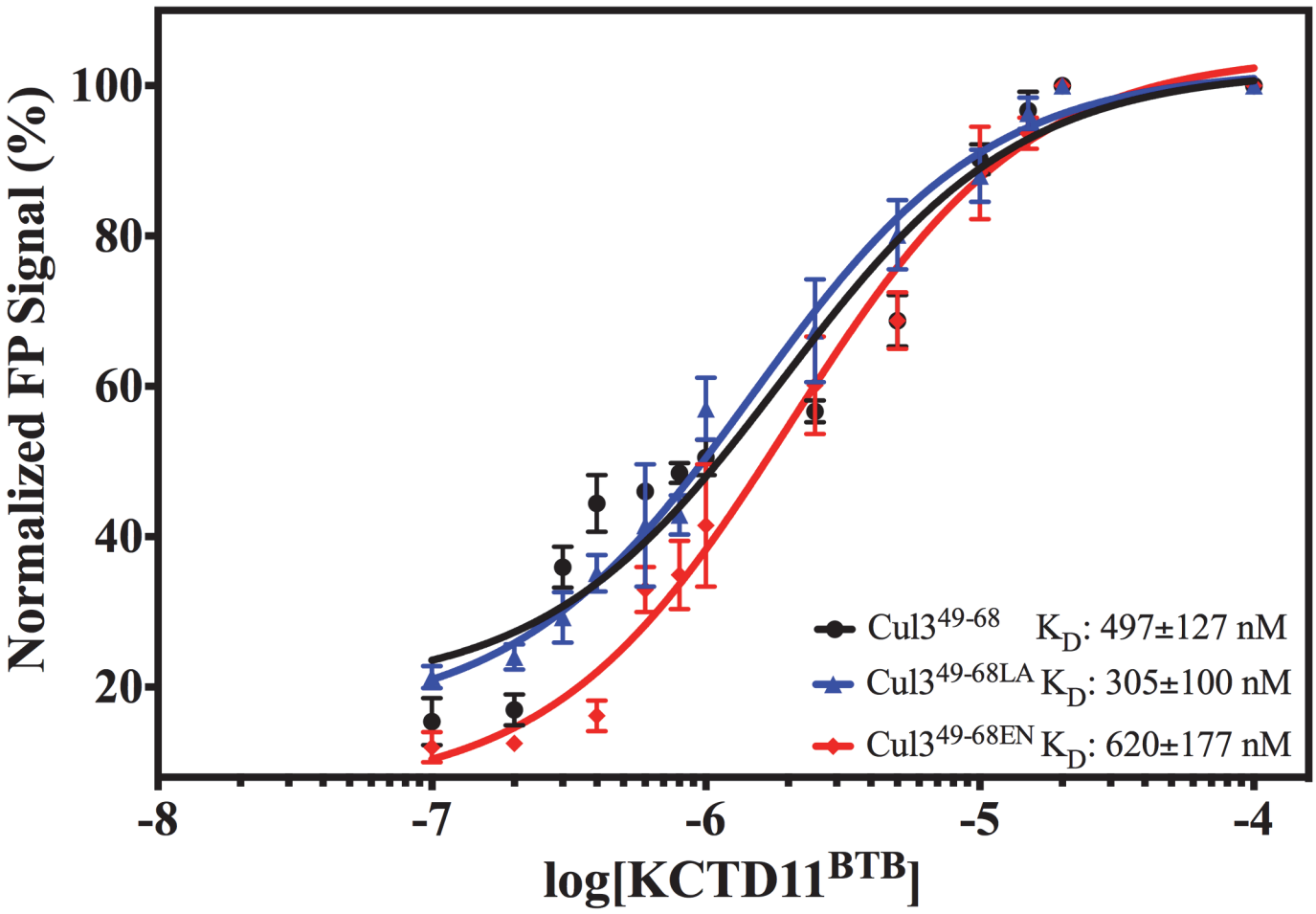

Fig 6. Normalized Fluorescence Polarization data for peptides as a function of [KCTD11^{BTB}]. Peptides were plated at a final concentration of 2 μM, and the interaction with KCTD11^{BTB} was tested over a concentration range of 0.1 nM to 20μM. Dissociation constants were calculated using nonlinear regression and are presented as mean ± standard error of triplicates.

doi:10.1371/journal.pone.0121149.g006

residues Leu52-Val65 and appears longer at the N-terminus than the Cul3$^{49\text{-}68EN}$ helix which is in turn longer at the C terminus spanning residues Phe54-His67. On the contrary, the overlay of a diagnostic portion of the NOESY spectrum of Cul3$^{49\text{-}68SL}$ with the same region of Cul3$^{49\text{-}68EN}$ spectrum shows the absence of the typical α-helix NOE connectivities in Cul3$^{49\text{-}68SL}$spectrum (S11 Fig.).

Serum stability of stapled peptides

The serum stability of the stapled peptides was monitored by LC/MS. It was found that the half-life of Cul3$^{49\text{-}68}$ in serum was 7h similarly to Cul3$^{49\text{-}68SL}$ whereas the half-lives of Cul3$^{49\text{-}68EN}$ and Cul3$^{49\text{-}68LA}$ increased to over 22h under the same conditions (Table 1). Mass spectra analysis indicates a preferential cleavage site at Tyr58 suggesting the presence of a chymotrypsin-like enzyme in the serum medium. Evidently, the presence of the hydrocarbon bridge reduces the accessibility of this residue in Cul3$^{49\text{-}68EN}$ and Cul3$^{49\text{-}68LA}$ compared to Cul3$^{49\text{-}68}$. On the other hand, the stapling between residues 53–57, as in Cul3$^{49\text{-}68SL}$, does not affect the accessibility of Tyr58. This observation is consistent with literature data reporting that the stapled

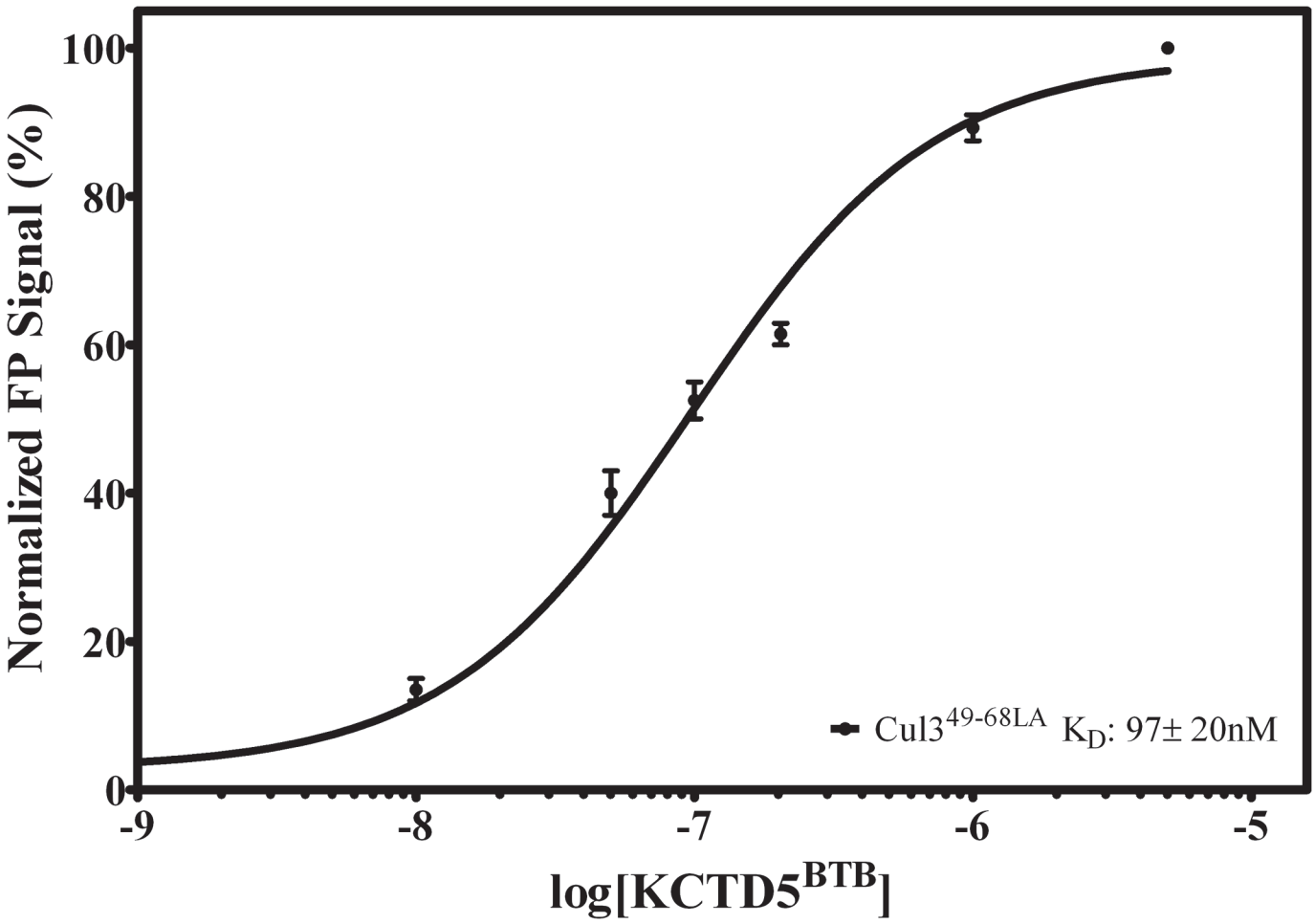

Fig 7. Normalized Fluorescence Polarization data for Cul3$^{49-68LA}$ as a function of [KCTD5^{BTB}]. Peptide was plated at a final concentration of 1 μM, and the interaction with KCTD5^{BTB} was tested over a concentration range of 0.1 nM to 5 μM. Dissociation constants were calculated using nonlinear regression and are presented as mean ± standard error of triplicates.

doi:10.1371/journal.pone.0121149.g007

peptides can be endowed with increased serum stability compared to the unmodified analogues [2].

Discussion

Cul3 is a large protein that is able to interact with a variety of different biological partners. The C-terminal region of the protein recruits, *via* the ring protein Rbx1, the E2 enzyme, whereas its N-terminal end anchors BTB-containing proteins that bring the substrate proteins to be ubiquitinated. Intriguingly, BTB-containing proteins that interact with Cul3 often present quite distinct features in terms of both sequence and oligomeric organization. Although other members of the cullin family have been the object of several structural characterizations, the first crystallographic studies on Cul3 have been reported only very recently [12]. These studies have provided interesting insights into the recognition mechanism of Cul3 by some dimeric BTB-containing proteins. In the last few years, an increasing attention has been devoted to an emerging class of potential Cul3-interacting proteins denoted as KCTDs, which are endowed with a larger structural complexity being able to associate in either pentameric or tetrameric states [46]. By combining experimental and theoretical approaches we have recently shown

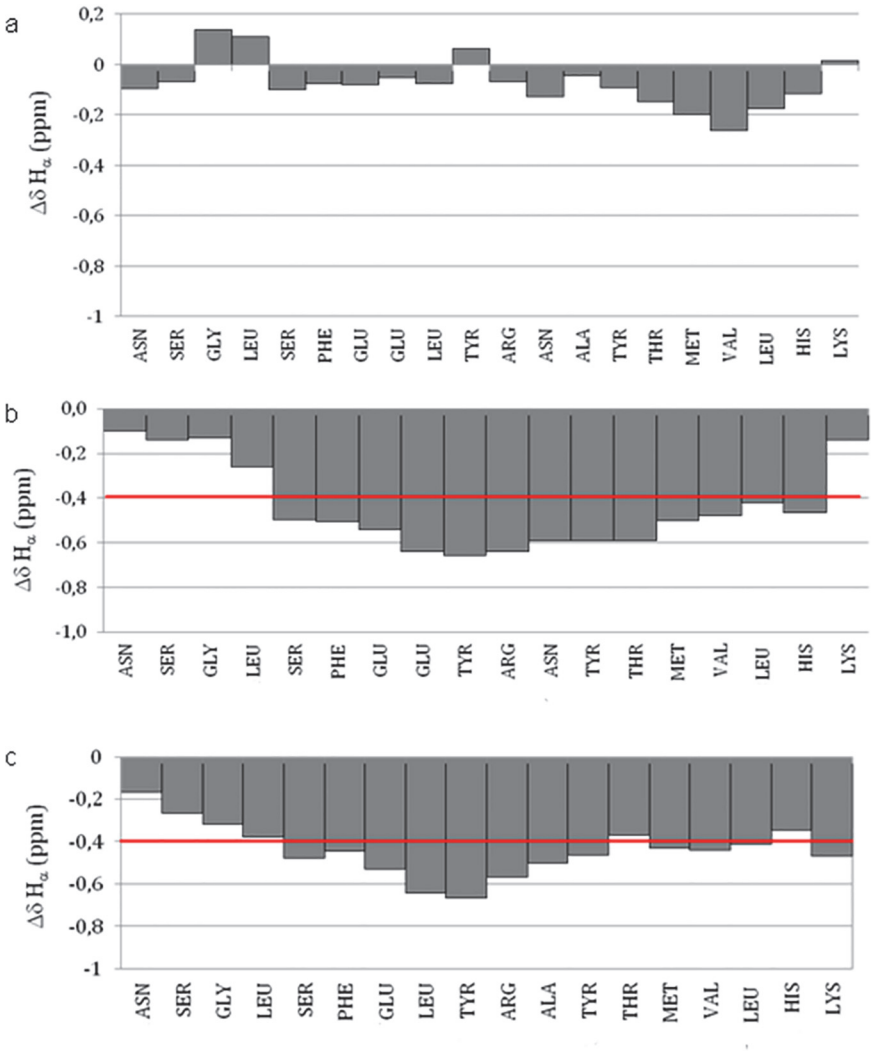

Fig 8. Hα secondary chemical shift for Cul3$^{49-68}$ (a), Cul3$^{49-68LA}$ (b) and Cul3$^{49-68EN}$ (c) peptides. The red line indicates the average upfield shifts observed in peptides database for α-helix.

doi:10.1371/journal.pone.0121149.g008

that the molecular recognition between KCTD5 and Cul3 involves a large surface area made of distinct hot spot regions located in the two proteins [34]. Nevertheless, in a preliminary study [16], we showed that a Cul3-based peptide, which comprises the fragment 49–68 of the protein, was able to bind two members of the family (a) the pentameric KCTD5 and (b) the tetrameric KCTD11. However, as shown in the present study, the use of this peptide as a biochemical tool or as a potential lead compound in therapeutic applications is seriously hampered by its limited stability in serum being highly susceptible to protease degradations. In order to improve the biochemical properties of Cul3-based peptides we designed, synthesized and characterized some stapled variants of the peptide [47]. In particular, MD simulations on the complex Cul3$^{49-68}$-KCTD11^{BTB} have highlighted that three aromatic residues (Phe54, Tyr58 and Tyr62) of the Cul3-derived peptide play a major role in KCTD11 recognition. These predictions have been corroborated by the observation that the peptide Cul3$^{49-68AA}$, in which Tyr58 and Tyr62 are replaced by Ala residues, is completely unable to bind KCTD11^{BTB} (Fig. 5). This finding corroborates and extends previous observations obtained by replacing these two Tyr with

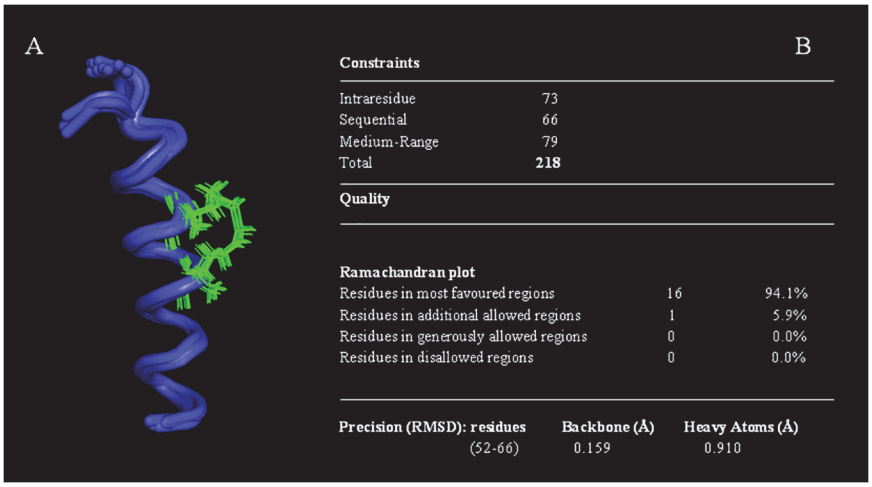

Fig 9. The NMR structure of Cul3$^{49\text{-}68EN}$. (A) NMR ensemble of the best 20 structures of Cul3$^{49\text{-}68EN}$ peptide. In the figure the *i*, *i* + *4* staple bridge produced by the combination of cross-linking (S)-2-(2'-pentenyl) alanine is shown in green. (B): Structural statistics for the Cul3$^{49\text{-}68EN}$ peptide.

doi:10.1371/journal.pone.0121149.g009

charged Lys residues [16]. Stapled peptides were therefore designed to make the local region of Phe54 or that of Tyr58 and Tyr62 more structured. The characterization of these variants clearly indicates that the impact of the stapling on the peptide structure and biochemical properties strongly depend on its location. Indeed, the stapling of the residues that are close to Phe54 (peptide Cul3$^{49\text{-}68SL}$) produces a very limited increase of the helical content (S10 Fig.). This observation may be explained by considering that the stapled region of Cul3$^{49\text{-}68SL}$ is located in the Cul3 structure at the very N-terminus of the helix 54–66. Therefore, this region is intrinsically less prone to adopt a helical state. The significant decrease of Cul3$^{49\text{-}68SL}$ affinity for KCTD11^{BTB} compared to the wild-type peptide indicates that the insertion of the stapling in this region likely perturbs the interactions of the peptide with the protein and that this

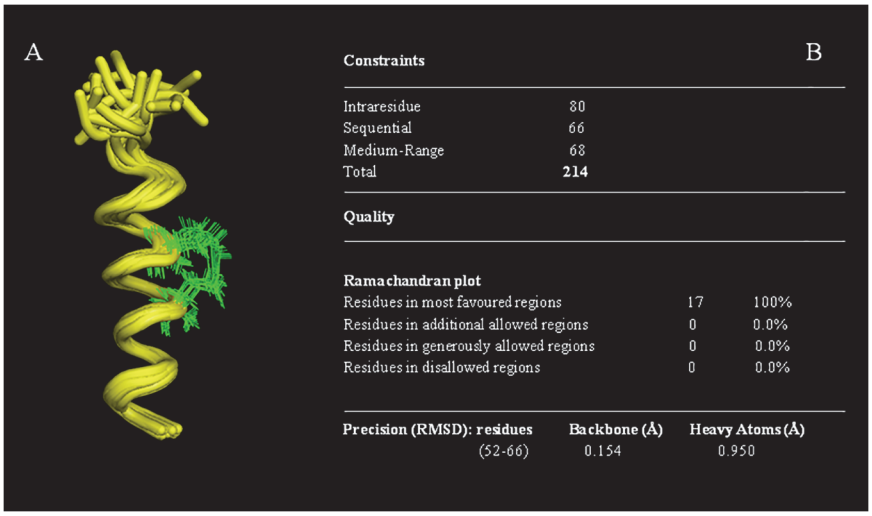

Fig 10. The NMR structure of Cul3$^{49\text{-}68LA}$. (A) NMR ensemble of the best 20 structures of Cul3$^{49\text{-}68LA}$ peptide. In the figure the *i*, *i* + *4* staple bridge produced by the combination of cross-linking (S)-2-(2'-pentenyl) alanine is shown in green. (B) Structural statistics for the Cul3$^{49\text{-}68LA}$ peptide.

doi:10.1371/journal.pone.0121149.g010

Table 1. Serum stability of the peptides and assignment of the fragments derived from proteolysis by LC/MS analysis.

PEPTIDE	ESTIMATE $t_{1/2}$	Fragment Mass (Da)	ASSIGNMENT
Cul3$^{49-68}$	~7h	1075	NAYTMVLHK-NH_2
		1355	Ac-NSGLSFEELYR
		1199	Ac-NSGLSFEELY
Cul3$^{49-68LA}$	~22h		n.d.
Cul3$^{49-68EN}$	~22h		n.d.
Cul3$^{49-68SL}$	~7h	1075	NAYTMVLHK-NH_2

doi:10.1371/journal.pone.0121149.t001

perturbation is not compensated by an increase of the helical content of the molecule. On the other hand, the stapling of the central region of the peptide has a different impact on the properties of Cul3$^{49-68}$. In particular, both Cul3$^{49-68LA}$ and Cul3$^{49-68EN}$ adopt well-defined, although slightly different, helical structures. Indeed, in Cul3$^{49-68LA}$ the α-helix encompasses the residues Leu52-Val65 whereas the one formed by Cul3$^{49-68EN}$ spans residues Phe54 to His67. The comparison of these helices with the helical region 54–66 of Cul3 clearly indicates that both are able to mimic the structure adopted by this region in the parent protein (Fig. 11). The superimposition of the helical region in Cul3 structure (PDB code 4EOZ) on Cul3$^{49-68EN}$ and Cul3$^{49-68LA}$ structures yields RMSD values, computed on the C^{α} atoms, of 1.10 and 0.83 Å, respectively. In addition, the relative orientation of the two interacting tyrosines (residues 58 and 62) with respect to the stapling bridge is, as expected, different in the two structures. These results indicate that the structure of Cul3$^{49-68LA}$ more closely resembles the structure found in Cul3. Although the two peptides both present affinities for KCTD11^{BTB} falling in the sub-micromolar range, some small differences have been detected. In particular, Cul3$^{49-68LA}$, whose structure is more similar to that exhibited by the helix in the parent protein, shows a slight increase in the affinity for KCTD11^{BTB} compared to the wild-type peptide. On the other hand, the stapling introduced in Cul3$^{49-68EN}$ marginally reduced the affinity for KCTD11^{BTB}. These findings indicate that the affinity of the stapled peptides limitedly correlates with their structural similarity with the helical region 54–66 of Cul3. Moreover, they also suggest that the increase of helical content does not necessarily reflect into increased affinity for KCTD11^{BTB}, as the hydrocarbon bridge of the stapling may perturb the proper protein-protein recognition mechanism.

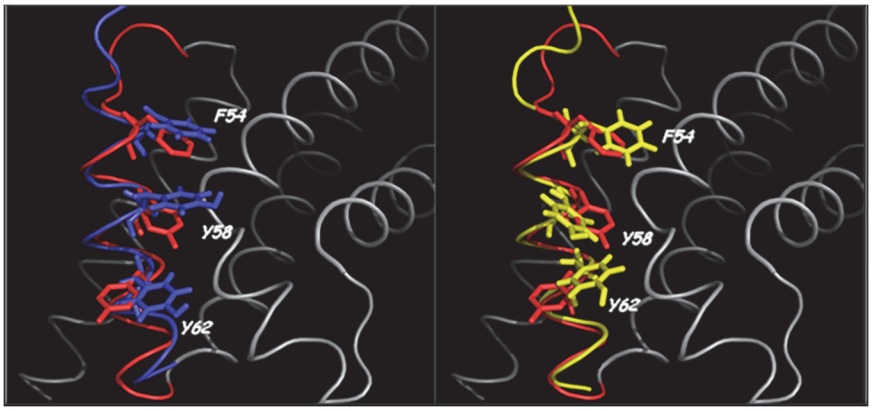

Fig 11. Superposition of the stapled peptides with Cul3. Superposition of the most representative conformer of Cul3$^{49-68EN}$ (left panel; blue) and Cul3$^{49-68LA}$ (right panel; yellow) respectively with the region (in red) encompassing residues Phe54-Leu66 of the crystal structure of Cul3 (PDB code 4EOZ).

doi:10.1371/journal.pone.0121149.g011

The insertion of the hydrocarbon bridge may lead to a significant increase of serum stability of these Cul3-derived peptides as both Cul3$^{49\text{-}68LA}$ and Cul3$^{49\text{-}68EN}$ display a higher resistance to degradation compared to the wild-type peptide. As for the affinity, the location of the stapling is essential for the peptide stabilization since present data show that Cul3$^{49\text{-}68SL}$ displays a serum stability comparable to the unmodified peptide. These findings suggest that the insertion of the stapling in the central region of Cul3$^{49\text{-}68}$ has a major impact on its biochemical and structural properties. It is important to note that the affinity displayed by Cul3$^{49\text{-}68LA}$ for KCTD11^{BTB} and for KCTD5^{BTB} is of the same order of magnitude of those reported for the interaction of Cul3 with some BTB containing proteins. Indeed, Cul3$^{49\text{-}68LA}$- KCTD11^{BTB} and Cul3$^{49\text{-}68LA}$- KCTD5^{BTB} affinities are intermediate between those exhibited by Cul3 for the BTB domain of SPOP [12] or of KCTD5 [34].

These considerations suggest that stapled peptides efficiently mimic these protein-protein interactions, although BTB-Cul3 recognition involves large and often non-contiguous, surfaces [48]. Therefore, taking also into account their serum stability, the stapled peptides we characterized are potentially able to modulate fundamental biological processes that involve a promiscuous and key protein such as Cul3. Notwithstanding the high performance of the stapled peptides, a further improvement in terms of solubility would be required for their applicability in clinical and experimental setups.

Supporting Information

S1 File. Generation of the KCTD11^{BTB} three-dimensional model; Protocol of the molecular dynamics simulation; Monitoring of the structure stability of the models along the trajectory.
(DOCX)

S1 Fig. Multiple sequence alignment of the BTB domains of different proteins. α-Helices and β-strands are denoted in blue and red, respectively.
(TIF)

S2 Fig. Evolution of (KCTD11^{BTB}-Cul3$^{49\text{-}68}$)$_4$ trajectory structures in simulation. (A) Root mean square deviations, computed using C$^{\alpha}$ atoms, compared to the starting model and (B) gyration radius.
(TIF)

S3 Fig. Root mean square fluctuations per residue of KCTD11^{BTB} and Cul3$^{49\text{-}68}$ in the equilibrated region of the trajectory. The lines reported in panels A represent residues in α-helices (cyan) or in β-sheets (red). In panel B, the helical residues of Cul3$^{49\text{-}68}$ are highlighted in cyan.
(TIF)

S4 Fig. Evolution of secondary structure in Cul3$^{49\text{-}68}$ in the simulation. Regions in blue, grey, yellow and green represent α-helices, 3–10 helices, turns and bends, respectively.
(TIF)

S5 Fig. Preserved intermolecular interactions along the trajectory. Examples of H-bonds and aromatic residues clustering are reported in panels A and B, respectively.
(TIF)

S6 Fig. Far-UV CD spectra of Cul3$^{49\text{-}68}$, Cul3$^{49\text{-}68EN}$, Cul3$^{49\text{-}68LA}$, and Cul3$^{49\text{-}68SL}$. Spectra were acquired in 0,1% TFA (pH 3.0).
(TIF)

S7 Fig. Dependence of Polarization signal of FITC-peptides as a function of [KCTD11^{BTB}].
(TIF)

S8 Fig. Dependence of Polarization signal of FITC-Cul3$^{49\text{-}68LA}$ as a function of [KCTD11^{BTB}].
(TIF)

S9 Fig. The ^{1}H NMR spectrum of Cul3 $^{49\text{-}68SL}$.
(TIF)

S10 Fig. Secondary Structure analysis. Summary of NMR parameters for Cul3$^{49\text{-}68EN}$ (A) and Cul3$^{49\text{-}68LA}$ (B). NOEs diagram, Chemical Shift Index (CSI) and Secondary Structure Propensities (SSP) are reported.
(TIF)

S11 Fig. Cul3$^{49\text{-}68SL}$. Overlay of a diagnostic portion of the NOESY spectrum of Cul3$^{49\text{-}68SL}$ peptide (Blue) with the same region of Cul3$^{49\text{-}68EN}$ spectrum (Red) showing in the case of Cul3$^{49\text{-}68SL}$ peptide the absence of the typical α-helix NOE connectivities.
(TIF)

S1 Table. ^{1}H chemical shifts for Cul3$^{49\text{-}68}$.
(DOCX)

S2 Table. ^{1}H chemical shifts for Cul3$^{49\text{-}68LA}$.
(DOCX)

S3 Table. ^{1}H chemical shifts for Cul3$^{49\text{-}68EN}$.
(DOCX)

S4 Table. Predictor results for Cul3$^{49\text{-}68EN}$ peptide.
(DOCX)

S5 Table. Predictor results for Cul3$^{49\text{-}68EN}$ peptide.
(DOCX)

Acknowledgments

We thank Luca De Luca for skilful technical support.

Author Contributions

Conceived and designed the experiments: IdP LP SDG GM LV EP LZ. Performed the experiments: IdP LP DM MP NB LE LR. Analyzed the data: IdP LP LDM SDG LV EP LZ. Contributed reagents/materials/analysis tools: SDG LV EP LZ. Wrote the paper: SDG LV EP LZ.

References

1. Blackwell HE, Grubbs RH. Highly efficient synthesis of covalently cross-linked peptide helices by ring-closing metathesis. Angew Chem Int Edit. 1998; 37(23):3281–4. PubMed PMID: ISI:000077806300017. English.
2. Verdine GL, Hilinski GJ. Stapled Peptides for Intracellular Drug Targets. Methods in Enzymology: Protein Engineering for Therapeutics, Vol 203, Pt B. 2012; 503:3–33. PubMed PMID: ISI:000300198000001. English.
3. Bird GH, Gavathiotis E, Labelle JL, Katz SG, Walensky LD. Distinct BimBH3 (BimSAHB) Stapled Peptides for Structural and Cellular Studies. ACS Chem Biol. 2014 Mar 21; 9(3):831–7. PMID: 24358963. Epub 2013/12/24. eng. doi: 10.1021/cb4003305

4. Joseph TL, Lane DP, Verma CS. Stapled BH3 Peptides against MCL-1: Mechanism and Design Using Atomistic Simulations. PLoS One. 2012 Aug 31; 7(8). PubMed PMID: ISI:000308221300039. English.
5. Bernal F, Tyler AF, Korsmeyer SJ, Walensky LD, Verdine GL. Reactivation of the p53 tumor suppressor pathway by a stapled p53 peptide. J Am Chem Soc. 2007 Apr 25; 129(16):5298–. PubMed PMID: ISI:000245782800073. English.
6. Moellering RE, Cornejo M, Davis TN, Del Bianco C, Aster JC, Blacklow SC, et al. Direct inhibition of the NOTCH transcription factor complex. Nature. 2009 Nov 12; 462(7270):182–8. PMID: 19907488. PMCID: 2951323. Epub 2009/11/13. eng. doi: 10.1038/nature08543
7. Walensky LD, Kung AL, Escher I, Malia TJ, Barbuto S, Wright RD, et al. Activation of apoptosis in vivo by a hydrocarbon-stapled BH3 helix. Science. 2004 Sep 3; 305(5689):1466–70. PMID: 15353804. PMCID: 1360987. Epub 2004/09/09. eng.
8. Phillips C, Roberts LR, Schade M, Bazin R, Bent A, Davies NL, et al. Design and structure of stapled peptides binding to estrogen receptors. J Am Chem Soc. 2011 Jun 29; 133(25):9696–9. PMID: 21612236. Epub 2011/05/27. eng. doi: 10.1021/ja202946k
9. Sviridov DO, Ikpot IZ, Stonik J, Drake SK, Amar M, Osei-Hwedieh DO, et al. Helix stabilization of amphipathic peptides by hydrocarbon stapling increases cholesterol efflux by the ABCA1 transporter. Biochem Biophys Res Commun. 2011 Jul 8; 410(3):446–51. PMID: 21672528. PMCID: 3253552. Epub 2011/06/16. eng. doi: 10.1016/j.bbrc.2011.05.154
10. Bhattacharya S, Zhang H, Debnath AK, Cowburn D. Solution structure of a hydrocarbon stapled peptide inhibitor in complex with monomeric C-terminal domain of HIV-1 capsid. J Biol Chem. 2008 Jun 13; 283(24):16274–8. PMID: 18417468. PMCID: 2423268. Epub 2008/04/18. eng. doi: 10.1074/jbc.C800048200
11. Pintard L, Willems A, Peter M. Cullin-based ubiquitin ligases: Cul3-BTB complexes join the family. Embo J. 2004 Apr 21; 23(8):1681–7. PMID: 15071497. PMCID: 394240. Epub 2004/04/09. eng.
12. Errington WJ, Khan MQ, Bueler SA, Rubinstein JL, Chakrabartty A, Prive GG. Adaptor protein self-assembly drives the control of a cullin-RING ubiquitin ligase. Structure. 2012 Jul 3; 20(7):1141–53. PMID: 22632832. Epub 2012/05/29. eng. doi: 10.1016/j.str.2012.04.009
13. Genschik P, Sumara I, Lechner E. The emerging family of CULLIN3-RING ubiquitin ligases (CRL3s): cellular functions and disease implications. Embo J. 2013 Aug 28; 32(17):2307–20. PMID: 23912815. PMCID: 3770339. Epub 2013/08/06. eng. doi: 10.1038/emboj.2013.173
14. Stogios PJ, Downs GS, Jauhal JJ, Nandra SK, Prive GG. Sequence and structural analysis of BTB domain proteins. Genome Biol. 2005; 6(10):R82. PMID: 16207353. PMCID: 1257465. Epub 2005/10/07. eng.
15. Canettieri G, Di Marcotullio L, Greco A, Coni S, Antonucci L, Infante P, et al. Histone deacetylase and Cullin3-REN(KCTD11) ubiquitin ligase interplay regulates Hedgehog signalling through Gli acetylation. Nat Cell Biol. 2010 Feb; 12(2):132–42. PMID: 20081843. Epub 2010/01/19. eng. doi: 10.1038/ncb2013
16. Pirone L, Correale S, de Paola I, Zaccaro L, De Simone G, Vitagliano L, et al. Design, synthesis and characterization of a peptide able to bind proteins of the KCTD family: implications for KCTD-cullin 3 recognition. J Pept Sci. 2011 May; 17(5):373–6. PMID: 21438081. Epub 2011/03/26. eng. doi: 10.1002/psc.1366
17. Correale S, Pirone L, Di Marcotullio L, De Smaele E, Greco A, Mazza D, et al. Molecular organization of the cullin E3 ligase adaptor KCTD11. Biochimie. 2011 Apr; 93(4):715–24. PMID: 21237243. Epub 2011/01/18. eng. doi: 10.1016/j.biochi.2010.12.014
18. Azizieh R, Orduz D, Van Bogaert P, Bouschet T, Rodriguez W, Schiffmann SN, et al. Progressive myoclonic epilepsy-associated gene KCTD7 is a regulator of potassium conductance in neurons. Mol Neurobiol. 2011 Aug; 44(1):111–21. PMID: 21710140. Epub 2011/06/29. eng. doi: 10.1007/s12035-011-8194-0
19. Di Marcotullio L, Ferretti E, De Smaele E, Argenti B, Mincione C, Zazzeroni F, et al. REN(KCTD11) is a suppressor of Hedgehog signaling and is deleted in human medulloblastoma. Proc Natl Acad Sci U S A. 2004 Jul 20; 101(29):10833–8. PMID: 15249678. PMCID: 490020. Epub 2004/07/14. eng.
20. Di Marcotullio L, Canettieri G, Infante P, Greco A, Gulino A. Protected from the inside: endogenous histone deacetylase inhibitors and the road to cancer. Biochim Biophys Acta. 2011 Apr; 1815(2):241–52. PMID: 21277938. Epub 2011/02/01. eng. doi: 10.1016/j.bbcan.2011.01.002
21. Williams MJ, Almen MS, Fredriksson R, Schioth HB. What model organisms and interactomics can reveal about the genetics of human obesity. Cell Mol Life Sci. 2012 Nov; 69(22):3819–34. PMID: 22618246. Epub 2012/05/24. eng. doi: 10.1007/s00018-012-1022-5
22. Golzio C, Willer J, Talkowski ME, Oh EC, Taniguchi Y, Jacquemont S, et al. KCTD13 is a major driver of mirrored neuroanatomical phenotypes of the 16p11.2 copy number variant. Nature. 2012 May 17; 485(7398):363–7. PMID: 22596160. PMCID: 3366115. Epub 2012/05/19. eng. doi: 10.1038/nature11091

23. Dementieva IS, Tereshko V, McCrossan ZA, Solomaha E, Araki D, Xu C, et al. Pentameric Assembly of Potassium Channel Tetramerization Domain-Containing Protein 5. J Mol Biol. 2009 Mar 20; 387 (1):175–91. PubMed PMID: ISI:000264610000014. English. doi: 10.1016/j.jmb.2009.01.030 PMID: 19361449

24. Bayon Y, Trinidad AG, de la Puerta ML, Del Carmen Rodriguez M, Bogetz J, Rojas A, et al. KCTD5, a putative substrate adaptor for cullin3 ubiquitin ligases. Febs J. 2008 Aug; 275(15):3900–10. PMID: 18573101. Epub 2008/06/25. eng. doi: 10.1111/j.1742-4658.2008.06537.x

25. Chen Y, Yang Z, Meng M, Zhao Y, Dong N, Yan H, et al. Cullin mediates degradation of RhoA through evolutionarily conserved BTB adaptors to control actin cytoskeleton structure and cell movement. Mol Cell. 2009 Sep 24; 35(6):841–55. PMID: 19782033. Epub 2009/09/29. eng. doi: 10.1016/j.molcel.2009.09.004

26. De Smaele E, Di Marcotullio L, Moretti M, Pelloni M, Occhione MA, Infante P, et al. Identification and characterization of KCASH2 and KCASH3, 2 novel Cullin3 adaptors suppressing histone deacetylase and Hedgehog activity in medulloblastoma. Neoplasia. 2011 Apr; 13(4):374–85. PMID: 21472142. PMCID: 3071086. Epub 2011/04/08. eng.

27. Hu X, Yan F, Wang F, Yang Z, Xiao L, Li L, et al. TNFAIP1 interacts with KCTD10 to promote the degradation of KCTD10 proteins and inhibit the transcriptional activities of NF-kappaB and AP-1. Mol Biol Rep. 2012 Nov; 39(11):9911–9. PMID: 22810651. Epub 2012/07/20. eng.

28. Huang T, Xu J, Xiang J, Lu Y, Chen R, Huang L, et al. PrPC interacts with potassium channel tetramerization domain containing 1 (KCTD1) protein through the PrP(51–136) region containing octapeptide repeats. Biochem Biophys Res Commun. 2012 Jan 6; 417(1):182–6. PMID: 22138399. Epub 2011/12/06. eng. doi: 10.1016/j.bbrc.2011.11.081

29. Bixby KA, Nanao MH, Shen NV, Kreusch A, Bellamy H, Pfaffinger PJ, et al. Zn2+-binding and molecular determinants of tetramerization in voltage-gated K+ channels. Nat Struct Biol. 1999 Jan; 6(1):38–43. PMID: 9886290. Epub 1999/01/14. eng.

30. Amadei A, Linssen AB, Berendsen HJ. Essential dynamics of proteins. Proteins. 1993 Dec; 17(4):412–25. PMID: 8108382. Epub 1993/12/01. eng.

31. Amadei A, Ceruso MA, Di Nola A. On the convergence of the conformational coordinates basis set obtained by the essential dynamics analysis of proteins' molecular dynamics simulations. Proteins. 1999 Sep 1; 36(4):419–24. PMID: 10450083. Epub 1999/08/18. eng.

32. Merlino A, Vitagliano L, Ceruso MA, Di Nola A, Mazzarella L. Global and local motions in ribonuclease A: a molecular dynamics study. Biopolymers. 2002 Nov 15; 65(4):274–83. PMID: 12382288. Epub 2002/10/17. eng.

33. Pirone L, Esposito C, Correale S, Graziano G, Di Gaetano S, Vitagliano L, et al. Thermal and chemical stability of two homologous POZ/BTB domains of KCTD proteins characterized by a different oligomeric organization. Biomed Res Int. 2013; 2013:162674. PMID: 24307990. PMCID: 3838848. Epub 2013/12/07. eng. doi: 10.1155/2013/162674

34. Balasco N, Pirone L, Smaldone G, Di Gaetano S, Esposito L, Pedone EM, et al. Molecular recognition of Cullin3 by KCTDs: Insights from experimental and computational investigations. Biochim Biophys Acta. 2014 Apr 18. PMID: 24747150. Epub 2014/04/22. Eng.

35. Kimple AJ, Yasgar A, Hughes M, Jadhav A, Willard FS, Muller RE, et al. A high throughput fluorescence polarization assay for inhibitors of the GoLoco motif/G-alpha interaction. Comb Chem High T Scr. 2008 Jun; 11(5):396–409. PubMed PMID: ISI:000256568700007. English.

36. Griesinger C, Otting G, Wuthrich K, Ernst RR. Clean Tocsy for H-1 Spin System-Identification in Macromolecules. J Am Chem Soc. 1988 Nov 9; 110(23):7870–2. PubMed PMID: ISI:A1988Q949000044. English.

37. Kumar A, Ernst RR, Wuthrich K. A two-dimensional nuclear Overhauser enhancement (2D NOE) experiment for the elucidation of complete proton-proton cross-relaxation networks in biological macromolecules. Biochem Biophys Res Commun. 1980 Jul 16; 95(1):1–6. PMID: 7417242. Epub 1980/07/16. eng.

38. Bartels C, Xia TH, Billeter M, Guntert P, Wuthrich K. The program XEASY for computer-supported NMR spectral analysis of biological macromolecules. J Biomol NMR. 1995 Jul; 6(1):1–10. PMID: 22911575. Epub 1995/07/01. eng. doi: 10.1007/BF00417486

39. Schwarzinger S, Kroon GJ, Foss TR, Wright PE, Dyson HJ. Random coil chemical shifts in acidic 8 M urea: implementation of random coil shift data in NMRView. J Biomol NMR. 2000 Sep; 18(1):43–8. PMID: 11061227. Epub 2000/11/04. eng.

40. Guntert P, Mumenthaler C, Wuthrich K. Torsion angle dynamics for NMR structure calculation with the new program DYANA. J Mol Biol. 1997 Oct 17; 273(1):283–98. PMID: 9367762. Epub 1997/11/21. eng.

41. Koradi R, Billeter M, Wuthrich K. MOLMOL: a program for display and analysis of macromolecular structures. J Mol Graph. 1996 Feb; 14(1):51–5, 29–32. PMID: 8744573. Epub 1996/02/01. eng.

42. Laskowski RA, Macarthur MW, Moss DS, Thornton JM. Procheck—a Program to Check the Stereochemical Quality of Protein Structures. J Appl Crystallogr. 1993 Apr 1; 26:283–91. PubMed PMID: ISI:A1993KY85100021. English.

43. Berjanskii MV, Neal S, Wishart DS. PREDITOR: a web server for predicting protein torsion angle restraints. Nucleic Acids Res. 2006 Jul 1; 34(Web Server issue):W63–9. PMID: 16845087. PMCID: 1538894. Epub 2006/07/18. eng.

44. Marsh JA, Singh VK, Jia ZC, Forman-Kay JD. Sensitivity of secondary structure propensities to sequence differences between alpha- and gamma-synuclein: Implications for fibrillation. Protein Sci. 2006 Dec; 15(12):2795–804. PubMed PMID: ISI:000242373700012. English. PMID: 17088319

45. Wishart DS, Sykes BD, Richards FM. The Chemical-Shift Index—a Fast and Simple Method for the Assignment of Protein Secondary Structure through Nmr-Spectroscopy. Biochemistry. 1992 Feb 18; 31 (6):1647–51. PubMed PMID: ISI:A1992HE19400010. English. PMID: 1737021

46. Liu ZP, Xiang YQ, Sun GH. The KCTD family of proteins: structure, function, disease relevance. Cell Biosci. 2013 Nov 24; 3. PubMed PMID: ISI:000331967800001. English.

47. Walensky LD, Bird GH. Hydrocarbon-Stapled Peptides: Principles, Practice, and Progress. J Med Chem. 2014 Mar 6. PMID: 24601557. Epub 2014/03/08. Eng.

48. Canning P, Cooper CD, Krojer T, Murray JW, Pike AC, Chaikuad A, et al. Structural basis for Cul3 protein assembly with the BTB-Kelch family of E3 ubiquitin ligases. J Biol Chem. 2013 Mar 15; 288 (11):7803–14. PMID: 23349464. PMCID: 3597819. Epub 2013/01/26. eng. doi: 10.1074/jbc.M112.437996